An Experimental and Detailed Kinetic Modeling of the Thermal Oxidation Stability of n-decane as a Jet Fuel Surrogate Component

M.D. Le, Z. El Sayah, R. Benrabah, V. Warth, P.-A. Glaude, R. Privat, R. Fournet, B. Sirjean

To cite this version:

M.D. Le, Z. El Sayah, R. Benrabah, V. Warth, P.-A. Glaude, et al.. An Experimental and Detailed Kinetic Modeling of the Thermal Oxidation Stability of n-decane as a Jet Fuel Surrogate Component. Fuel, 2023, 342, pp.127754. 10.1016/j.fuel.2023.127754 . hal-03996643

HAL Id: hal-03996643
https://hal.science/hal-03996643v1

Submitted on 20 Feb 2023

HAL is a multi-disciplinary open access archive for the deposit and dissemination of scientific research documents, whether they are published or not. The documents may come from teaching and research institutions in France or abroad, or from public or private research centers.

L'archive ouverte pluridisciplinaire **HAL**, est destinée au dépôt et à la diffusion de documents scientifiques de niveau recherche, publiés ou non, émanant des établissements d'enseignement et de recherche français ou étrangers, des laboratoires publics ou privés.

An Experimental and Detailed Kinetic Modeling of the Thermal Oxidation Stability of *n*-decane as a Jet Fuel Surrogate Component

M.D. Le,[1] Z. El Sayah,[1] R. Benrabah,[1] V. Warth,[1] P.-A. Glaude,[1] R. Privat,[1] R. Fournet,[1] B. Sirjean[1,*]

[1] Université de Lorraine, CNRS, LRGP, F-54000 Nancy, France

Corresponding author:

Baptiste Sirjean

Laboratoire Réactions et Génie des Procédés

1 rue Grandville BP 20451 54001 Nancy Cedex, France

Email: baptiste.sirjean@univ-lorraine.fr

Abstract

Thermal oxidation stability of liquid jet fuels remains a significant scientific challenge in the development of modern aviation. This study aims at experimentally and numerically investigating the autoxidation of *n*-decane, which is used as a component of jet fuel surrogates in the literature. Induction periods (IP) of *n*-decane were measured in a PetroOxy device under 7 bar of oxygen and cell temperatures varying from 403 to 418 K. IPs give a quantitative measure of the oxidation stability of a fuel. In addition to IPs measurements, the total hydroperoxides content at the end of the IP test was quantified using two iodometric titration methods: colorimetry and potentiometry. In order to simulate the oxidation of the homogeneous liquid phase as a batch reactor, we developed a physical model based on the so-called gamma-phi thermodynamic approach to calculate the compositions of liquid- and gas-phases at the set temperatures and pressures. Based on a state-of-the-art method to capture solvent effects, a detailed kinetic model for the *n*-decane autoxidation was developed. The simulations are consistent with experimental data from this study (IP and hydroperoxides concentration profiles) and from the literature. The proposed model is validated to simulate the thermal oxidation stability of liquid *n*-decane, for conversions up to 15%. Kinetic analyzes highlight the central role played by hydroperoxides decomposition and the self-termination of peroxy decyl (ROO·) radicals in the autoxidation of *n*-decane.

1. **Introduction**

The rapid growth of worldwide aviation requires intense research efforts to optimize aircraft engines to achieve better energy efficiency and emission reductions [1]. Aviation liquid fuels, also called jet fuels, are used as the main energy carrier in aircraft engines but also have a role in the cooling system, which is specific to them [2]. Indeed, if their primary role is to provide energy through the combustion in jet engines, their second role is to act as a coolant, which ensures the normal operation of several parts including, the hydraulic and the lubrication systems, the combustor and the airframe and environmental control system [2]. Due to their use as a heat sink, jet fuels undergo thermal stresses [3]. For example, in commercial aircrafts, it can be exposed to temperature of 393 to 433 K for several seconds under cruise conditions [4-6]. During their logistic operations, from their storage to the jet engine injectors, jet fuels are in contact with air under various pressure and temperature conditions. Dissolved oxygen from air in the fuel promotes the liquid phase oxidation of the fuel, also called autoxidation. This phenomenon is the source of major issues in aircrafts as it forms undesired products including gums and deposits. Nowadays, the formulation of jet fuels, including additives, allows them to remain stable throughout their use as coolant in commercial aircrafts, but to temperatures up to 433 K [4]. In order to increase the efficiency of future turbine engines and design supersonic aircrafts operating at higher speed it is necessary to improve the thermal oxidation stability of jet fuel so that it can be stable up to temperatures as high as ≈573 K [7]. Comprehensive studies on jet fuel autoxidation are therefore essential to understand, predict and optimize their thermal oxidation stability.

Jet fuels are blends of hundreds of hydrocarbons. To facilitate jet fuel studies, including numerical and experimental works, researchers proposed several jet fuel surrogates [8]. A jet fuel surrogate is a mixture of pure compounds combined to mimic physical and ignition characteristics of real jet fuels. *n*-decane is commonly used as a mono-component surrogate or included in multi-component surrogate for jet fuels [9-12]. Thus, the development of a kinetic model of autoxidation of *n*-decane, validated against experiments, is a first step towards a jet fuel surrogate kinetic model. Kinetic modelling of *n*-decane autoxidation is also of great interest to understand lubricant degradation [13]. This remains a challenge in the literature as liquid phase detailed kinetic models are at their early stages of developments compared to gas-phase models [14, 15]. It is commonly accepted in the community that both gas-phase oxidation and liquid-phase oxidation of hydrocarbons undergo similar radical mechanisms [15]. While the gas-phase oxidation mechanism of large alkanes such as *n*-decane is well understood [16], its liquid-phase oxidation mechanism remains to be fully understood [2].

Several studies on *n*-decane autoxidation have been performed in the literature. Cullis et al. [17] performed *n*-decane liquid and gas phases oxidation experiments in the same temperature region. They found some notable differences in the mechanisms in the two phases: absence of C_{10} O-heterocycles and dihydroperoxides in the liquid phase and small amounts of lower mass oxygenated compounds, compared to gas phase experiments. Experiments on the slow combustion of *n*-decane were performed in a closed reactor between 445 and 473 K and liquid phase oxidation was conducted in a semi-open reactor in which a flux of oxygen was passed into an isothermal batch reactor at 423 K containing *n*-decane. Principal products of *n*-decane autoxidation were determined as decane monohydroperoxides, C_{10} carbonyls and alcohols.

Goosen and Morgan [18] studied the products obtained during the autoxidation of *n*-decane and *n*-nonane, at significant conversion. Oxygen was passed into boiling *n*-decane, in a reflux, at about 451 K. In the investigated conditions, these authors described the autoxidation of *n*-decane as proceeding in three stages: the first stage involves the formation of alkyl hydroperoxides, the second stage occurs when the hydroperoxide decomposes into alcohols and ketones, and the last stage corresponds to the oxidation of the latter products in competition with the alkanes, yielding γ-lactones and carboxylic compounds.

Pfaendtner and Broadbelt [13, 19] used automated mechanism generation to study the autoxidation of *n*-decane to understand lubricant oil degradation. They proposed condensed phase adapted rate rules and kinetic parameters, based on structure reactivity correlations, and were able to simulate the autoxidation of *n*-decane and *n*-octane and validated the results against experimental data of the literature. This pioneering work was the first to use detailed chemical kinetic modeling to simulate the liquid phase oxidation of alkanes. However, it is entirely based on gas-phase thermochemical data and most of the kinetic data adopted are based on gas-phase estimations.

Recently, Chatelain et al. [20] investigated the autoxidation kinetic of several *n*-alkanes including *n*-decane by conducting Induction Periods (IP) measurements at three different temperatures (393, 413, and 433 K) in a PetroOxy device. Liquid-phase mechanisms of these alkanes were generated thanks to an automated mechanism generator, RMG [21], and were capable of predicting IP within a factor of 3 at high temperature (T > 413 K). Note that only the autoxidation kinetic models of *n*-octane and *n*-dodecane are available from this study.

Auzani et al.[22] assessed the effect of ethanol on the IPs of a real kerosene and three surrogates. They proposed a Python code to simulate the pressure drop in the PetroOxy measurements that solves the ordinary differential equations of a Perfectly Stirred Reactor for each species and an equation for the consumption of the number of moles of O_2 in the gas phase. RMG was used to generate detailed reaction mechanisms for *n*-decane, ethanol and *n*-dodecane and simulate some of their experimental results. Upon significant changes in the kinetic data of the $R\cdot + O_2$ reactions, they were able to qualitatively simulate their experimental results. The same group also proposed a skeletal kinetic mechanism for liquid hydrocarbons autoxidation to simulate experiments on a fuel composed of five normal alkanes in a near-isothermal reactor and in a PetroOxy device [23].

The motivations of our study are: (1) to provide additional experimental data for the liquid-phase reactivity of *n*-decane; (2) to define a rigorous framework to model IP data measured in PetroOxy devices; (3) to develop a validated kinetic model of *n*-decane autoxidation and (4) to refine the understanding of *n*-decane autoxidation. To reach these goals, IPs of *n*-decane were measured in a

PetroOxy and were coupled with an experimental quantification of the total hydroperoxides (ROOH) content. These data allow us to define a rigorous criterion for the simulation of IPs which is based on the total amount of ROOH in the aged fuel. The kinetic model of *n*-decane was developed using our reaction mechanism generator (EXGAS [24, 25]) which has been adapted to automatically capture solvent effects on the thermochemical data based on corrections computed with an Equation of State (EoS) [26, 27]. This approach has been validated in the case of the liquid-phase oxidation of *n*-butane [26]. The main reaction pathways of *n*-decane liquid-phase oxidation are presented and discussed in this paper.

This work will contribute to improve the experimental kinetic studies performed in PetroOxy on jet fuels because a method to determine the liquid-vapor equilibrium in the test cell is proposed for the first time. A new approach to determine the IP from homogeneous liquid phase simulations is also proposed, based on ROOH quantification. Finally, a new detailed kinetic model is proposed, based on the calculation of hundreds of new thermochemical data adapted to *n*-decane solvent and new reaction rate rules. This model is systematically validated against all available literature data. This model will constitute a building block for the construction of detailed multi-component jet fuel surrogate models which are necessary to understand the oxidation stability of jet fuels and to allow the optimization and formulation of future aviation energy carriers.

2. Experimental methods

2.1. PetroOxy description

Experiments of *n*-decane autoxidation were conducted in a PetroOxy, a device that has been widely used for fuel stability studies [28-31] and employed as a reference instrument in ASTM D7525, ASTM D7545 and EN 16091 tests [32]. A PetroOxy apparatus operates similarly as a closed batch reactor: it contains a gold-plated test cell, whose volume is 25 mL. The experiment begins with the introduction of 5 ml of fuel into the cell, which is then pressurized under 7 bar of pure oxygen. High-purity *n*-decane (⩾99%) from Sigma-Aldrich were employed in this work. The reactor is then heated quickly (about 3 minutes) from the ambient to the desired temperature and kept constant until the end of the test. The temperature in these tests ranged from 403 to 418 K. The gas-phase pressure is followed during each experiment and, as the autoxidation of *n*-decane consumes oxygen, a decrease of pressure is observed. The induction period (IP) is defined as the time corresponding to a 10% pressure drop from the maximum pressure reached at the beginning of the test (as illustrated in Figure 1).

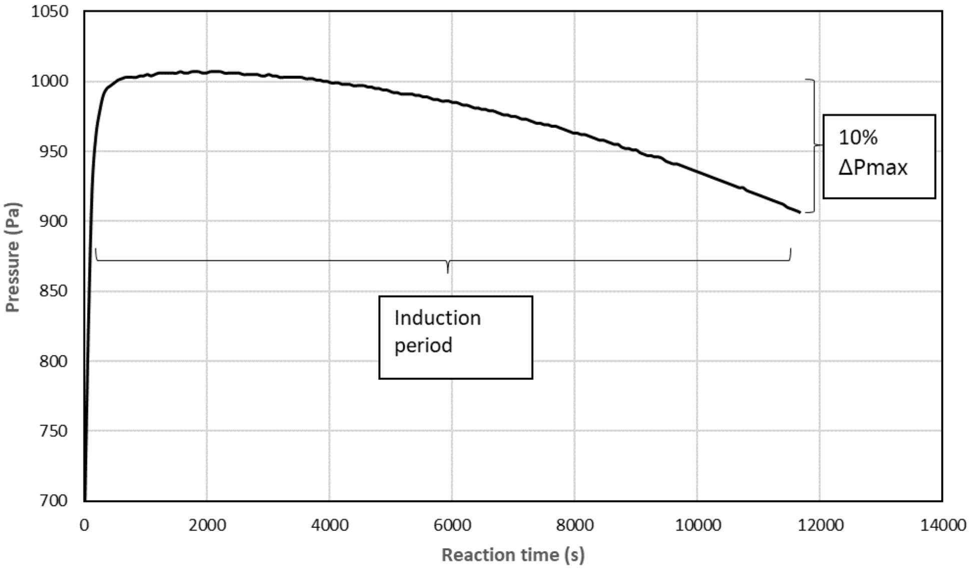

Figure 1. Evolution of measured pressure during a typical PetroOxy test and definition of the induction period (IP) Fuel: n-decane, test temperature: 413 K, initial O_2 pressure: 7 bar.

The IP characterizes the thermal oxidation stability of a fuel and decreases with increased oxidation rates of the fuels. The maximum uncertainty observed for our experimental induction periods is 10% of IP at the lowest temperature (403 K). This uncertainty was ascribed to all measured IPs (see Table S1).

2.2. Hydroperoxide quantification: iodometric method

Since the simulations of the autoxidation process are performed in a homogeneous liquid-phase reactor with a constant oxygen content [14, 20, 26], it is difficult to directly simulate the, gas-phase, pressure decrease measured in the PetroOxy. In the literature [20, 33], the definition of the IP in the simulations was assumed to correspond to a conversion of 5% of the fuels oxidized in the PetroOxy. However, the extent of fuel conversion at IP is fuel dependent definition is not universal and Mielczarek et al. [34] indicated that the conversion of toluene at corresponding IP was around 40%. In this work, we propose to link the IP with another experimental measure: the total hydroperoxides content at the IP. This creates a universal criterion to define the IP in the simulations, where the simulated IP is reached when the simulated total content of ROOH matches the experimental one. To quantify the total hydroperoxides concentration, two methods based on iodometric titration were used in this study.

2.2.1. Colorimetry

The iodometric titration method developed by Roohi and Rajabi [35] was used to quantify the total hydroperoxides content in aged fuels at the end of each PetroOxy test. The main advantage of this method, compared to the classic titration that uses thiosulfate in aqueous solution as titrant [36, 37], resides in the use of triphenylphosphine diluted in *n*-decane as titrant. Solubility issues of *n*-decane in water are therefore avoided in the titrant. The titration was performed in two steps:

1) the first step involves the oxidation of iodide anion I^- to iodine I_2 by hydroperoxides at a temperature of 68 °C. A volume of 1 ml of aged *n*-decane, sampled at the end of the IP in the PetroOxy, was added to a solution of potassium iodide (KI, anhydrous 99.9%, VWR Chemicals) and acetic acid (≥ 99.8 %, Sigma Aldrich) in absolute ethanol (≥99.8%, VWR Chemicals). The reaction is presented in equation (1). The resulting solution has a yellow-reddish color of iodine.

$$\mathbf{ROOH + 2H^+ + 2I^- \rightarrow I_2 + ROH + H_2O} \qquad (1)$$

(Colorless) (Yellow-reddish)

2) The second step involves the titration of the iodine with triphenylphosphine (TPP, 99 %, Sigma Aldrich), which produce an uncolored complex $[TPPI]^+[I]^-$, as presented in equation (2). The color change at the endpoint is therefore provided by the complexation of iodine. TPP was prepared in a solution of pure *n*-decane (99+%, ACROS Chemicals) at a concentration of 0.08 mol/L. The titration endpoint point was determined as a sharp color change was observed.

$$\mathbf{I_2 + TPP \rightarrow [TPPI]^+[I]^-} \qquad (2)$$

(yellow-reddish) (colorless)

The uncertainty of the concentration of ROOH with the colorimetric titration depends mainly on the uncertainty of the volume of the titration endpoint, which comes from different sources of errors: the reading of the burette, the uncertainty of the burette (given by the constructor), and the manipulations. The detection limit of the equivalence point depends on the size of the drop of the burette which is 0.05 mL. The uncertainty calculations are presented in details in the supplementary material. The uncertainty in equivalence volumes determined via colorimetry is ±0.14 mL, with a confidence interval of 95%.

2.2.2. Potentiometry

As colorimetry, potentiometry is used to quantify I_2 after the iodometric reaction. The biggest difference between two methods is the considered indicator which is a sharp color change in iodometric titration and a sharp electric potential change in potentiometric titration. Potentiometry has been shown to improve the method for measuring hydroperoxides in fuels, thanks to a better determination of the endpoint compared to the visual detection of the color change in standard titration [36]. The electric potential during the titration of I_2 was followed by a Mettler Toledo Compact Titrator G10S.

As for the colorimetry, the uncertainty on the final ROOH concentration obtained by potentiometry method mainly depends on the uncertainty of the titration endpoint volume. The use of a potentiometer allows a better detection of end points because of lowest size of the drops of the burette. Despite the uncertainty on the measured potential (given by the constructor) the global uncertainty in the titration endpoint volume remains well below the uncertainty of the colorimetric titration with a value of ±0.04 mL, with a confidence interval of 95% (see Table S2 for more details).

3. Kinetic modelling

3.1. Detailed kinetic model development

In a recent work [26], we presented an approach to develop a detailed kinetic model for fuel autoxidation based on the corresponding gas-phase kinetic model. In order to capture solvent effects, it is essential to include thermodynamic, diffusion and kinetic corrections. The details of the method can be accessed in the work on *n*-butane autoxidation kinetics [26], and only the most important features are recalled here.

The first step in the development of the detailed chemical kinetic model for the autooxidation of *n*-decane was the generation of the low-temperature oxidation (gas-phase) kinetic mechanism, using the EXGAS software [24, 25]. This software has been extensively used and validated for the computer aided generation of combustion kinetics models of hydrocarbons and oxygenated fuels [24, 38-42]. The generated mechanism is composed of three parts: a primary and a secondary mechanism and a C_0-C_2 reaction basis. In the primary mechanism, all the possible elementary reactions of the reactants, and free radicals produced, are written and leads to a large number of primary products. If the primary molecular products are larger than C_2, their decomposition reactions are generated and are lumped to yield C_0-C_2 products in order to avoid an excessive growth of the size of the mechanism. For products lower than C_2, the combustion reactions are included in the exhaustive C_0-C_2 reaction base. The details of the adaptation of the *n*-decane gas-phase model to the liquid-phase is described hereafter.

3.1.1. Thermochemical data

The gas-phase thermochemical data for all the species that do not belong to the C_0-C_2 reaction base were generated using the THERGAS code [43] based on Benson group additivity method [44]. C_0-C_2 species thermochemistry is taken form literature databases. The gas-phase data are then corrected by $\Delta_{sol}G(T)$ calculated at infinite dilution, using the equation of state (EoS) universal mixing rule Peng-Robinson UNIFAC (UMR-PRU) [45] to obtain the liquid-phase thermochemical data. Further details of $\Delta_{sol}G(T)$ calculation can be accessed elsewhere [26, 27, 46].

3.1.2. Liquid-phase kinetic data

The typical reaction pathways occurring during the oxidation of an alkane in the liquid phase, at low conversion, can be schematized as in Figure 2 [47].

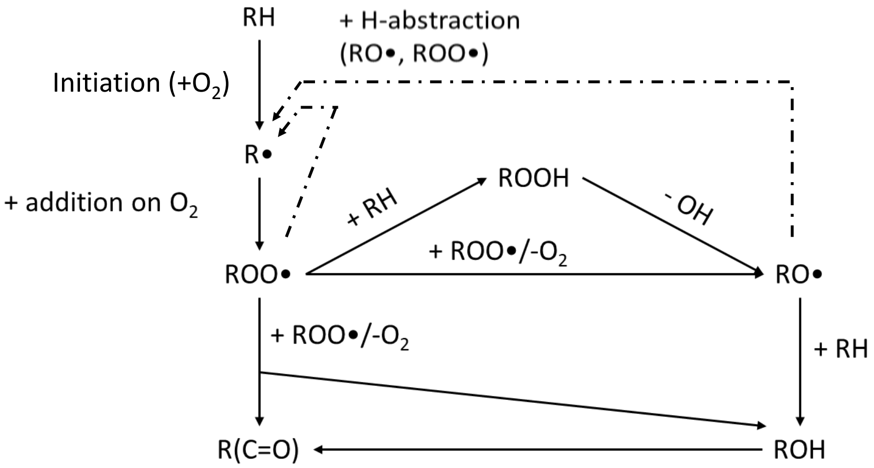

Figure 2. Simplified reaction pathways of an alkane in the liquid phase

The main consumption channels of the reacting alkane (RH) are H-atom abstractions by peroxy radical (ROO•) and alkoxy radical (RO•), all yielding the main alkyl radical R•. The latter radical produces the corresponding peroxy radical ROO• upon addition on dissolved O_2. One of the main reactions of peroxy radical ROO• yields the corresponding peroxide ROOH via H-atom abstractions from the reactant. The remaining consumption route of this radical involves the self-reactions (ROO• + ROO•) that produce an alcohol (ROH) and a ketone (or aldehyde) (R(C=O)) in a termination step (disproportionation) known as Russell mechanism, or two alkoxy radical RO• and O_2. Hydroperoxide ROOH entirely decomposes into two radicals, an alkoxy radical RO•, and a hydroxyl radical •OH. This degenerate branching reaction is the most important reaction governing the liquid-phase reactivity of alkanes as it transforms a molecule into two reactive radicals. ROH is produced by both self-termination reactions of peroxide radical ROO• and H-atom abstraction of the reactant RH by the alkoxy radical RO•. This alcohol ROH is then oxidized into ketone (or aldehyde) R(C=O) by successive reactions, which follow a similar pattern as the one for alkanes autooxidation.

The reaction classes in this model are bimolecular initiations, additions of alkyl radicals on oxygen, radical decompositions by beta-scission, H-atom abstractions from the reactant by radicals, and disproportionation. It can be noted that internal isomerization of ROO• radicals are negligible in alkanes autoxidation [17, 48] and that this reaction class can be ignored in the reaction mechanism [13, 26]. A set of new reaction rate rules, adapted to the liquid-phase oxidation of *n*-decane, was established for the self-termination reactions of peroxy radicals, and the H-atom abstractions by peroxy and alkoxy radicals based on the corresponding reactions in the autoxidation model of *n*-butane [26]. For the other reactions, the EXGAS reaction rate rules were adopted as the simulations demonstrated that they are not sensitive for *n*-decane conversion and for the products formation. The most important features of the developed mechanism are presented below.

3.1.2.1 *Initiations and beta-scissions*

Bimolecular initiations involve the reactions R1-R5 of *n*-decane (n-$C_{10}H_{12}$) with O_2. Five isomers of *n*-decyl radicals (1-$C_{10}H_{21}$, 2-$C_{10}H_{21}$, 3-$C_{10}H_{21}$, 4-$C_{10}H_{21}$, 5-$C_{10}H_{21}$) are produced. The kinetic parameters were taken from EXGAS rate rules (for a primary H-atom, (R1): $k = 4.2 \times 10^{13} \times \exp(-53033 \text{ cal mol}^{-1}/RT)$ $cm^3 mol^{-1} s^{-1}$; for a secondary H-atom (R2-R5) : $k = 2.8 \times 10^{13} \times \exp(-50650 \text{ cal mol}^{-1}/RT)$ $cm^3 mol^{-1} s^{-1}$). The influence of diffusive rate constants on these kinetic parameters were verified and were found to be negligible. This point is further discussed in the 3.1.3 section.

n-$C_{10}H_{22} + O_2 = 1\text{-}\bullet C_{10}H_{21} + HO_2$ (R1)
n-$C_{10}H_{22} + O_2 = 2\text{-}\bullet C_{10}H_{21} + HO_2$ (R2)
n-$C_{10}H_{22} + O_2 = 3\text{-}\bullet C_{10}H_{21} + HO_2$ (R3)
n-$C_{10}H_{22} + O_2 = 4\text{-}\bullet C_{10}H_{21} + HO_2$ (R4)
n-$C_{10}H_{22} + O_2 = 5\text{-}\bullet C_{10}H_{21} + HO_2$ (R5)

In the condition of low temperature oxidation, only C-C bond β-scissions free radicals were considered. Via reactions R6-R14, decyl radicals produce smaller alkenes and alkyl radicals.

$1\text{-}\bullet C_{10}H_{21} = \bullet C_8H_{17} + C_2H_4$ (R6)

$2\text{-}\bullet C_{10}H_{21} = \bullet C_7H_{15} + C_3H_6$ (R7)

$3\text{-}\bullet C_{10}H_{21} = \bullet C_6H_{13} + C_4H_8$ (R8)

$3\text{-}\bullet C_{10}H_{21} = \bullet CH_3 + C_9H1_8$ (R9)

$4\text{-}\bullet C_{10}H_{21} = \bullet C_5H_{11} + C_5H_{10}$ (R10)

$4\text{-}\bullet C_{10}H_{21} = \bullet C_2H_5 + C_8H_{16}$ (R11)

$5\text{-}\bullet C_{10}H_{21} = \bullet C_3H_7 + C_7H_{14}$ (R12)

$5\text{-}\bullet C_{10}H_{21} = \bullet C_4H_9 + C_6H_{12}$ (R13)

EXGAS rate rules were used to estimate the kinetic data of β-scissions. Only two structure-reactivity correlations are needed as reactions (R6-R13) falls within two reaction classes: R• → alkene + $\bullet C_{x>2}H_{2x+1}$ ($k_{6,7,8,10,11,12,13}$) = 2.0 x10^{13} x exp(-28700/RT)) and R• → alkene + $\bullet CH_3$ (k_9 = 2.0 x10^{13} x exp(-31000/RT)) in cm^3, mol, cal, K, s units.

3.1.2.2 Additions on oxygen and oxidations

The five decyl radicals ($C_{10}H_{21}$) reacts with O_2 to give decyl peroxy radicals, $C_{10}H_{21}OO\bullet$ (R14-R18). EXGAS rate rules were adopted for these reactions with the rate constant k_s = 1.8 x10^{19} x $T^{-2.5}$ for the addition of secondary radical onto O_2 (R15-R18) and k_p = 9.0 x10^{18} x $T^{-2.5}$ in the case of the primary decyl radical (R14), in cm^3, mol, cal, K, s units. Diffusivities were calculated for these reactions (see 3.1.3) and were found to be negligible.

$1\text{-}\bullet C_{10}H_{21} + O_2 = 1\text{-}C_{10}H_{21}OO\bullet$ (R14)

$2\text{-}\bullet C_{10}H_{21} + O_2 = 2\text{-}C_{10}H_{21}OO\bullet$ (R15)

$3\text{-}\bullet C_{10}H_{21} + O_2 = 3\text{-}C_{10}H_{21}OO\bullet$ (R16)

$4\text{-}\bullet C_{10}H_{21} + O_2 = 4\text{-}C_{10}H_{21}OO\bullet$ (R17)

$5\text{-}\bullet C_{10}H_{21} + O_2 = 5\text{-}C_{10}H_{21}OO\bullet$ (R18)

In the model, the additions on O_2 of the decyl radicals compete with the oxidation reactions, which consist in the oxidation of decyl radicals by oxygen to form decene (R19-R23). All decene isomers were lumped into one species ($C_{10}H_{20}$) to reduce the complexity of the model.

$1\text{-}\bullet C_{10}H_{21} + O_2 = C_{10}H_{20} + HO_2$ (R19)

$2\text{-}\bullet C_{10}H_{21} + O_2 = C_{10}H_{20} + HO_2$ (R20)

$3\text{-}\bullet C_{10}H_{21} + O_2 = C_{10}H_{20} + HO_2$ (R21)

$4\text{-}\bullet C_{10}H_{21} + O_2 = C_{10}H_{20} + HO_2$ (R22)

$5\text{-}\bullet C_{10}H_{21} + O_2 = C_{10}H_{20} + HO_2$ (R23)

EXGAS rate rules were used for the kinetic data.

3.1.2.3 H-atom abstractions

H-atom abstractions are the principal consumption flux of *n*-decane in liquid-phase oxidation, yielding five *n*-decyl radicals. These reactions involve the transfer of a H-atom from *n*-decane to radicals that are present in significant amounts. In our mechanism, these radicals are: hydroxyl (OH), hydroperoxyl (HO_2), methyl ($\bullet CH_3$), methoxy ($CH_3O\bullet$), methyl peroxy ($CH_3OO\bullet$), five isomers of decoxy radicals ($C_{10}H_{21}O\bullet$) and five isomers of *n*-decyl peroxy radicals ($C_{10}H_{21}OO\bullet$). In the model, the five isomers of *n*-decanol were lumped as $C_{10}H_{21}OH$ and the five isomers of *n*-decyl hydroperoxide were lumped as $C_{10}H_{21}OOH$. In the experiments of *n*-decane liquid-phase oxidation [17, 20], decanol was determined as one of the major products. Most H-atom abstractions follow EXGAS rate rules except H-atom abstractions by alcoxy and peroxy radicals, which were shown to be very sensitive in *n*-butane autoxidation. In the model of *n*-decane, the rate constants of H-atom abstractions by C_{10} peroxy radicals are estimated using an analogy with the H-abstraction from *n*-butane by butylperoxy radicals [26]. The kinetic parameters of H-atom abstraction by C_{10} alkoxy radicals were estimated by analogy with H-atom abstractions of *n*-butane by C_4 alkoxy radicals based on theoretical calculations with an implicit continuum solvation model.

3.1.2.4 Disproportionations

Disproportionations are known as chain-terminating processes. In the model, these reactions are included for all important peroxy radicals. For example, decyl peroxy react with HO_2 as $ROO\bullet + HO_2 \rightarrow ROOH + O_2$. Kinetic parameters of these reactions follow EXGAS rate rules.

Another type of disproportionation considered in the model is the self-terminations of decyl peroxy radicals. This reaction class is known crucial processes in the autoxidation of alkanes [13, 26, 48]. The self-termination of C_{10} peroxy radicals has two exit channels: (1) producing two decoxy radicals ($C_{10}H_{21}O\bullet$) and O_2, and (2) producing O_2, C_{10} alcohols and C_{10} carbonyl compounds. In our model, isomers of C_{10} carbonyl compounds were lumped as $C_{10}H_{20}OK$. For these two reaction classes, kinetic parameters were proposed as $k_1 = 1.0 \times 10^{11} \times \exp(2700\ \text{cal mol}^{-1}/RT)\ \text{cm}^3\ \text{mol}^{-1}\ \text{s}^{-1}$, $k_2 = 2.0 \times 10^{11} \times \exp(2700\ \text{cal mol}^{-1}/RT)\ \text{cm}^3\ \text{mol}^{-1}\ \text{s}^{-1}$. The ratio $\alpha = k_1 / k_2$ is 0.5. It has been shown in *n*-butane liquid-phase oxidation [26] that the ratio α could be between 0.5 and 1 to get reasonable simulation results. It is interesting to note that a ratio α=1 was used in the *n*-butane kinetic model to obtain the best agreement between simulations and experiments. In the case of *n*-decane, the ROO• + ROO• → RO• + RO• + O_2 channel is favored over the ROO• + ROO• → ROH + R_1COR_2 + O_2 by a factor of 2. It is difficult to find an explanation for this difference, it can be either a meaningful physical effect or a consequence of the lumping of the C_{10} alcohols and C_{10} carbonyl compounds. Indeed, in the *n*-butane autoxidation model, no lumping of alcohols and ketones was used.

3.1.2.5 Decompositions of hydroperoxides

The unimolecular decompositions of hydroperoxides (ROOH) plays an important role as these processes generate free radicals (RO• and OH). The rate constant of the decomposition of *n*-decyl hydroperoxide is $k = 1.60 \times 10^{11} \times \exp(-31700/RT)$ in mol, cal, K, s units. This rate constant results from a regression analysis of experimental data reported in the review of Dixon [49].

3.1.2.6 Decanol sub-mechanism

Decanol is one of the major products quantified experimentally in *n*-decane liquid-phase oxidation [17, 20]. To limit the size of the mechanism, a simplified sub-mechanism was developed for decanol, following the validated approach used for butanol in the autoxidation model of *n*-butane [26]. In the model, the lumped alcohol $C_{10}H_{21}OH$ is consumed by H-abstraction by decyl peroxy (ROO•) and OH radicals to produce an α-hydroxyl alkyl (•ROH) radical noted as RC10H21OL. In this approach, the H-abstraction is assumed to solely occur on the α-site of the hydroxyl group because of a lower C-H bond dissociation energy at this position compared to other H-atoms of decanol. The •ROH radical is then oxidized by O_2 to form lumped C_{10} carbonyl compounds and HO_2. The associated rate constants are estimated using the proposed rate rules in the *n*-butane model [26].

3.1.3. Diffusion correction

To account for diffusive limits in the liquid phase, a diffusion rate constant (k_{diff}) has to be combined to the intrinsic liquid-phase constant ($k_{int,liq}$). This leads to the following effective rate constant (k_{eff}) for a bimolecular reaction A+B ⇆ (A-B) → *Products*:

$$k_{eff} = \frac{k_{diff} \times k_{int,liq}}{k_{diff} + k_{int,liq}}$$

k_{diff} was calculated using the Stokes-Einstein approach for diffusion of spherical particles in the liquid phase [14, 26]. In this approach, molecular radii of considered species are calculated based on the UNIFAC molecular size parameter included in UMR-PRU equation of state [27]. Temperature-dependent viscosities are read in a literature database [50]. Diffusion calculations were conducted for all the most important bimolecular reactions included in the main reaction flux of *n*-decane. It is found that the values of k_{diff} are nearly similar for the different considered reactions and increase with temperatures. k_{diff} varies from 4×10^{13} at 300 K to about 2×10^{16} cm^3 $mole^{-1}$ s^{-1} at 500 K. As the values of k_{diff} of the considered reactions are very high because of the relatively low viscosity of *n*-decane (0.29 mPa.s at 400 K), k_{eff} = $k_{int,liq}$. A similar behavior was observed for *n*-butane which has a much lower liquid viscosity (0.005 mPa.s at 400 K).

3.2. Calculation of liquid and gas phases initial compositions in the PetroOxy

The simulation of liquid-phase oxidation in the PetroOxy is performed using a homogeneous batch reactor model at fixed temperature (T), pressure (P) and volume (V) and with a constant dissolved O_2 concentration [14, 20, 26]. In the input, T is the target temperature (e.g. 140°C) that is used to accelerate the oxidation phenomena. However, in the PetroOxy experiments, the 25 mL cell is first filled with 5 mL of *n*-decane and sealed under atmospheric air pressure. The cell is then purged and filled with 7 bar of O_2 at ambient temperature and heated to the target temperature. With the increasing temperature, the compositions of the liquid and gas phases evolve. It can be noted that the heating time to reach the control temperature is a few minutes.

In conjunction with the temperature increase, the pressure in the cell test increases from the initial value at 25°C (700 kPa) to a maximum value. Several competing physical phenomena affect the pressure evolution, including the thermal expansion, the evaporation of the fuel, and the solvation of oxygen in the liquid phase. An iterative calculation method has been developed to estimate molar compositions of both liquid and gas phases in a PetroOxy test, when the gas pressure reaches its maximum pressure. These molar compositions were used as inputs in IP simulations. Figure 3 presents the simplified boundary conditions that needs to be considered in the calculations.

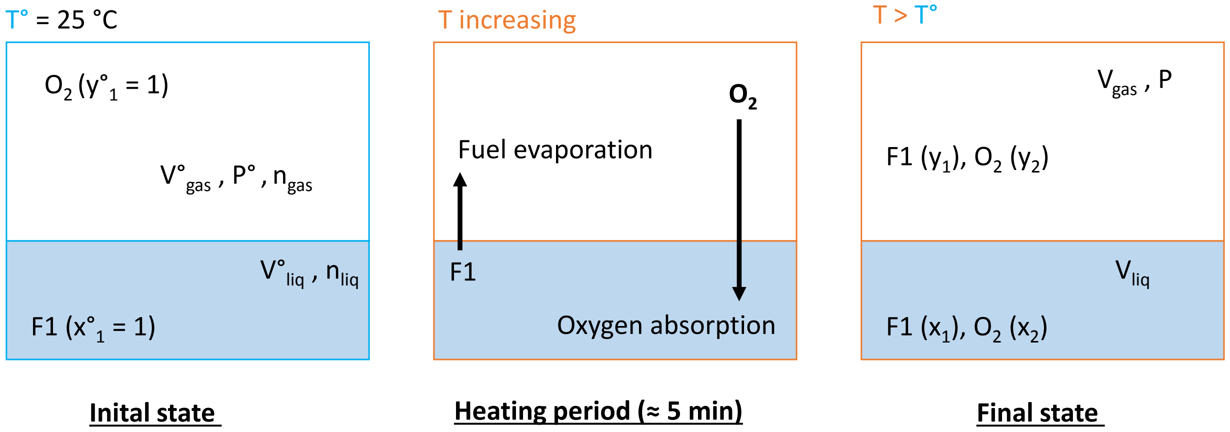

Inital state **Heating period (≈ 5 min)** **Final state**

Figure 3. Simplified scheme presenting the different steps when the temperature increases in the PetroOxy.

In Figure 3, F1 is the fuel, x_n and y_n are the mole fractions of the compound *n* (1 for the liquid fuel and 2 for oxygen) in the liquid and gas phases, respectively. In the initial state (T° = 25 °C), it is assumed that the gas phase contains only oxygen (O_2, $y°_2 = 1$) and the initial gas pressure (P°) is equal to the initial oxygen pressure ($P^{initial}_{O2}$ = 7 bar). Similarly, the liquid phase is composed only of fuel (F1, $x°_1 = 1$). The initial volume of the liquid phase, noted $V°_{liq}$, is 5 mL. The transient state, represented at the center of Figure 3, corresponds to the heating phase of the reactor and the final state corresponds to the thermodynamic equilibrium at the test temperature.

The system obeys the laws of conservation during the temperature increase: volume conservation ($V_{gas} + V_{liq} = V_{total}$ = 25 mL = constant) and the material balance:

$$\text{Overall balance: } \mathrm{n_{gas}} + \mathrm{n_{liq}} = \mathrm{n_{total}} = \text{ constant}$$
$$\text{Balance on component } i\text{: } \mathrm{n_{gas,i}} + \mathrm{n_{liq,i}} = \mathrm{n_{total,i}} = \text{ constant}$$

where n_{gas} and n_{liq} are the mole number of the gas and liquid phases, respectively; $\mathrm{n_{gas,i}}$ and $\mathrm{n_{liq,i}}$ are the mole number of the component *i* in the gas and liquid phases.

The total volume of the gas phase obeys the perfect gas law, $V_{gas} = \frac{RT}{P}(n_{gas,1} + n_{gas,2})$. The total volume of the liquid phase is deduced from the density of the liquid (D_{liq}) phase, $V_{liq} = \frac{n_{liq,1}M_1 + n_{liq,2}M_2}{D_{liq}(T, x_1, x_2)}$.

In the final state, both the gas and liquid phases contain mixtures of the fuel F1 and oxygen. The molar compositions of both phases and the final pressure (P) are related and are described using the so-called $\gamma - \varphi$ thermodynamic approach in which the liquid solvent is assumed to obey Raoult's law while the liquid solute is described using Henry's law; the gas phase is considered as a perfect gas. These assumptions are justified as long as (i) the molar fraction of the solvent in the liquid phase is nearly one ($x_1 \to 1$), (ii) the molar fraction of the liquid solute approaches zero ($x_2 \to 0$) and (iii), the total pressure remains below 10 bar (ensuring that the perfect-gas assumption is acceptable).

$$P \times y_1 = P_1^{sat} \times x_1 \quad (1)$$
$$P \times y_2 = H_{O2} \times x_2 \quad (2)$$

P_1^{sat} corresponds to the vapor pressure of the pure fuel F1 and H_{O2} is the Henry's law constant of oxygen in F1 solvent. Both these properties depend on temperature only.

Remembering that $x_i = \frac{n_{liq,i}}{n_{liq,1} + n_{liq,2}}$ and $y_i = \frac{n_{gas,i}}{n_{gas,1} + n_{gas,2}}$ $(i = 1,2)$, the final problem to be solved is summarized in the following system, gathering 5 equations:

$$\begin{cases} P \times y_1 = P_1^{sat}(T) \times x_1 & (1) \\ P \times y_2 = H_{O2}(T) \times x_2 & (2) \\ V_{total} = \dfrac{n_{liq,1}M_1 + n_{liq,2}M_2}{D_{liq}(T, x_1, x_2)} + \dfrac{RT}{P}(n_{gas,1} + n_{gas,2}) & (3) \\ & (4) \\ n_{total,i} = n_{liq,i} + n_{gas,i}, \qquad i = 1,2 & (5) \end{cases}$$

$T, V_{total}, n_{total,1}, n_{total,2}$ are input variables. The 5 unknowns are $P, n_{gas,1}, n_{gas,2}, n_{liq,1}, n_{liq,2}$.

In practice, the resolution of Eq. (1-5) is carried out using successive substitution methods. The proposed iterative calculation method consists of several steps and is presented in Figure 4. In the first step, a gas pressure in the final state is guessed based on the ideal gas law, assuming constant mole number and volume of the gas phase. Next, molar composition in the liquid phase is deduced thanks to the conservation of volume, material balance and relations (1) and (2). The thermodynamic properties involved in these equations, *i.e.*, the liquid density (D_{liq}), vapor pressure (P^{sat}), Henry's law constant of oxygen (H_{O2}) in solvent, are obtained from the Predictive SRK (PSRK) equation of state [51] implemented in Simulis software [52]. The PSRK model, capable of guesstimating the above properties, was chosen for both its flexibility and accuracy.

At the end of a calculation process, the sum of molar composition in the liquid phase is checked whether it is equal to 1. A tolerance of 0.005 is adopted. If the checking condition is not satisfied, a new liquid density and gas pressure are estimated and the calculation loop starts again until the validation of the checking condition.

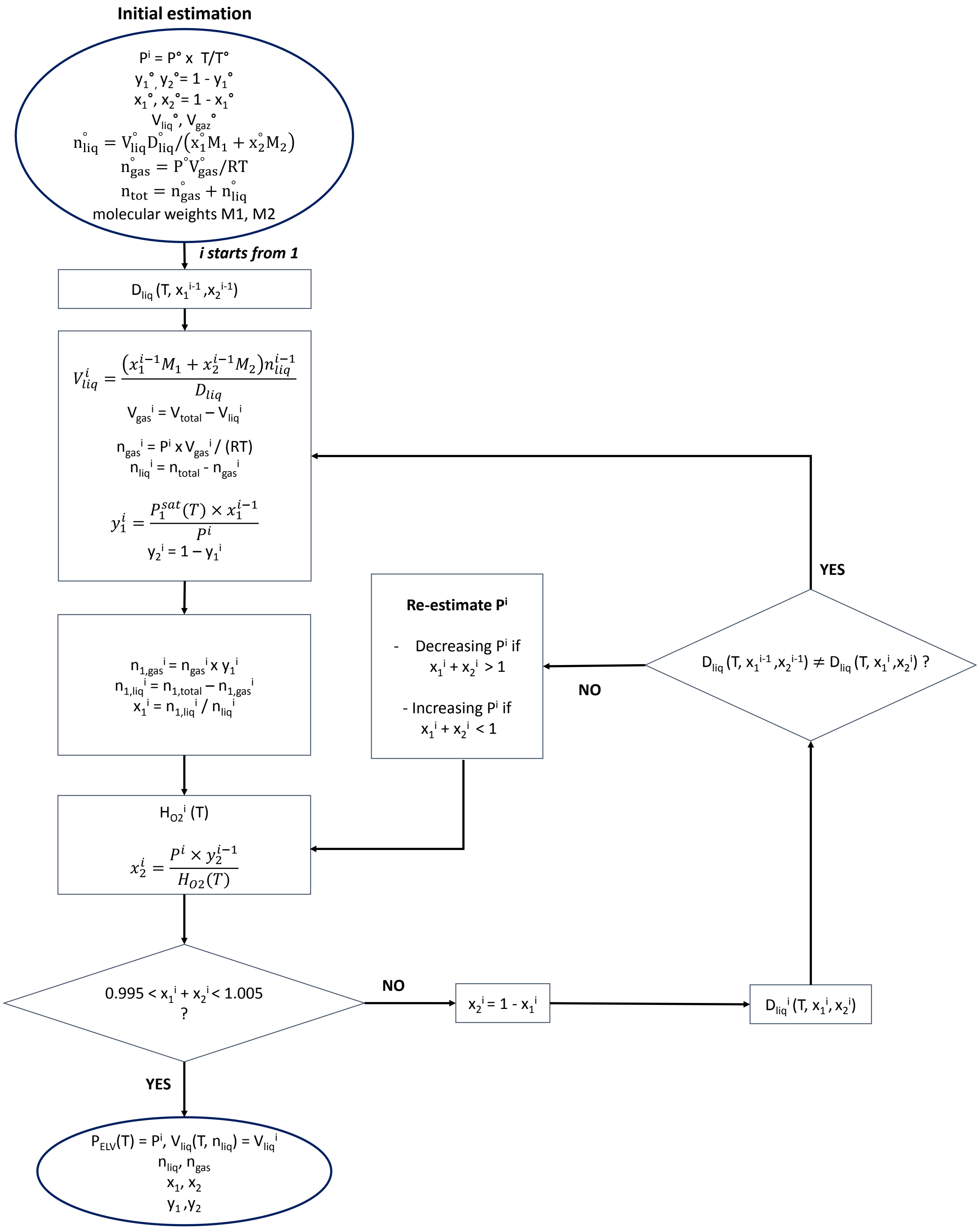

Figure 4. Iterative calculation method to estimate the maximum pressure and molar composition in PetroOxy experiments

The iterative calculation presented in Figure 4 was used to determine the initial composition at the set temperature T in the PetroOxy experiments. This method enables the simulation of the gas pressure profiles as a function of temperature at the beginning of the tests, until the maximum pressure is reached (Figure 5).

Figure 5. Simulations of pressure profiles as a function of time at the beginning of PetroOxy tests (heating phase up to the set temperature T) of *n*-decane at different T: (a) 403 K, (b) 408 K, (c) 413 K, (d) 418 K. Symbols are experimental data and solid lines are simulated pressure profiles. Experimental pressure profiles of heating phases are given in Table S3.

In general, simulations reproduce the measured pressure profiles and are able to capture the equilibrium between the liquid and vapor phases.

The physical model predicts that at the end of the heating time of 5 minutes, the volume of liquid increases from 5.0 to 5.7 mL, going from 298 to 413 K. At 413 K, the mole fractions of *n*-decane and dissolved O_2 in the liquid phase are 0.98 and 0.02, respectively. For this condition, the corresponding gas-phase mole fractions are 0.04 for *n*-decane and 0.96 for O_2.

The mole compositions of the liquid phase corresponding to the maximum gas pressure are also determined, at different temperatures (Table 1).

Table 1. Calculated molar composition of the liquid phase corresponding to the maximum gas pressure during PetroOxy tests of n-decane.

Cell temperature (K)	**[*n*-Decane] (mol/L)**	**[Oxygen] (mol/L)**
403	4.51	8.56×10^{-2}
408	4.48	8.56×10^{-2}
413	4.45	8.75×10^{-2}
418	4.41	8.97×10^{-2}

The calculated compositions were used as concentration inputs to simulate the induction periods of *n*-decane at different temperatures. It is interesting to note that the calculated concentration of O_2

dissolved in *n*-decane increases with temperature. A similar behavior is well known for O_2 in jet fuels [6]. All the simulations were performed using a homogeneous liquid batch reactor (constant T, P, and V) solver based on Chemkin II library [53] with constant O_2 concentration [14, 26, 34].

4. Results and Discussions

Experimental results in PetroOxy are first presented, then, the simulations and the performances of the *n*-decane autoxidation model are shown. Based on the validated model, the reaction pathways of *n*-decane autoxidation are analyzed and the key reactions are highlighted thanks to a sensitivity analysis.

4.1. Liquid-phase reactivity of *n*-decane

Figure 6 presents the measured induction periods of *n*-decane as a function of the inverse of the temperature. The IP of *n*-decane measured in this work are consistent with the data reported by Chatelain et al. [20].

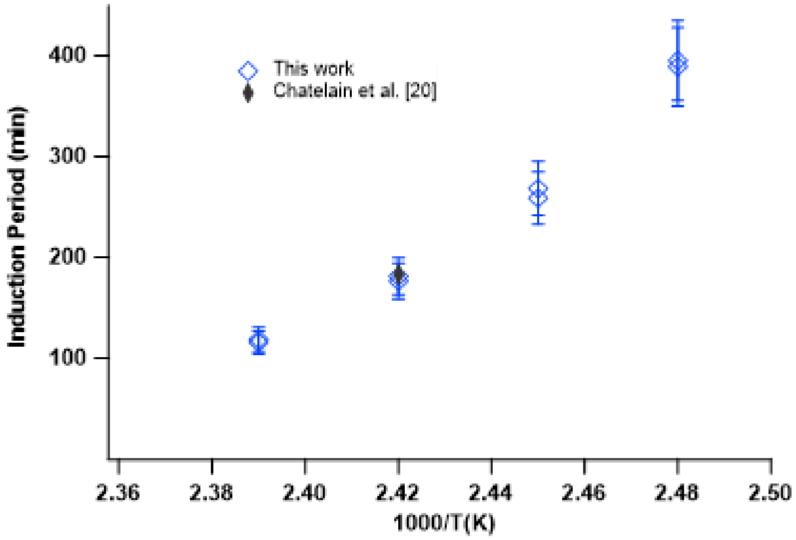

Figure 6. Induction periods of n-decane measured in a PetroOxy at 7 bar initial of oxygen and comparison with data reported by Chatelain et al. [20].

Total hydroperoxides content in aged *n*-decane was quantified by iodometry, using colorimetric and potentiometric titrations. The measured hydroperoxide (ROOH) concentrations at the IP time are presented as a function of the PetroOxy cell temperature in Figure 7. IP and [ROOH] data are given in Table S4 and S5.

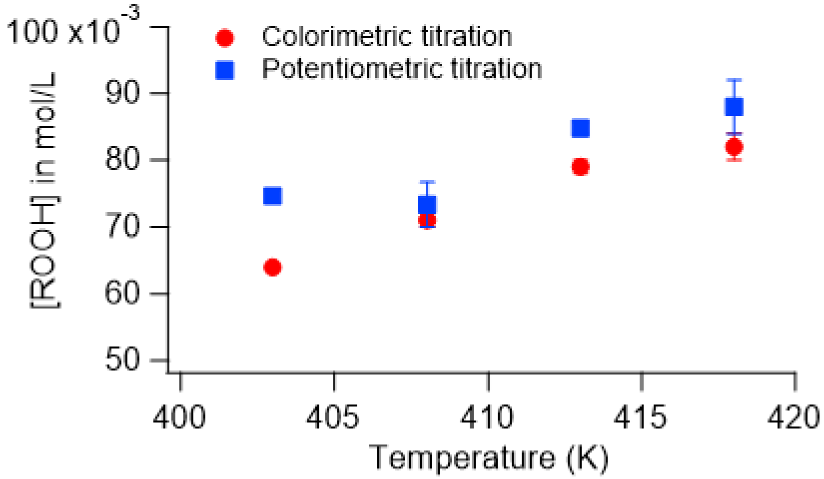

Figure 7. Total hydroperoxides content in *n*-decane, at IP (experiments at 7 bar initial of O_2), measured by colorimetric and potentiometric titrations. Error bars are the repeatability standard deviations.

Both endpoint detection methods indicate that the ROOH concentration increases with temperature. The ROOH concentrations obtained from potentiometry are generally higher than those measured by colorimetry by a about 5 x 10^{-3} mol l^{-1}. Our uncertainty calculations showed that potentiometric titration is more accurate than colorimetric titration since an electronic signal is used in the former method (see Table S2). Consequently, the potentiometric total ROOH concentrations were used as the criterion to determine the IP time in the simulation: the simulated IP is reached when the simulated total concentration of ROOH matches the experimental one.

Figure 8 presents the simulation of measured IP of *n*-decane in this work using the liquid-phase kinetic model developed.

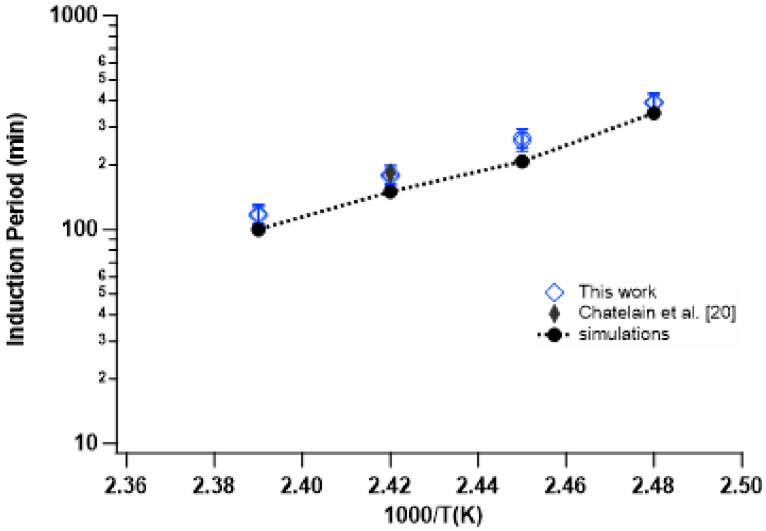

Figure 8. Comparison between simulated and experimental induction periods of *n*-decane in a PetroOxy device, at 7 bar of oxygen. Criteria for simulated IP: simulated $[ROOH]_{total}$ = $[ROOH]_{total}$ measured at IP.

Under the investigated conditions, the measured IP of *n*-decane presented in logarithmic scale varies nearly linearly with the inverse of reactor temperatures. The simulation reproduces experimental results with a mean relative deviation of 16% over the temperature range studied. Further validations of the kinetic model were performed using oxidation products profiles.

For one condition of oxidation stability test, at 413 K and 7 bar of oxygen, the total concentration of ROOH as a function of time was measured. To do so, PetroOxy tests were stopped every *t* = t(previous test) + 15 min until the IP time was reached (Figure 9). The total [ROOH] content was measured by potentiometric titration. The titration of fresh, unaged, *n*-decane revealed that the liquid already contained hydroperoxides at a concentration of 0.016 mol/L. This initial hydroperoxides content was also employed as inputs in all simulations of *n*-decane autoxidation.

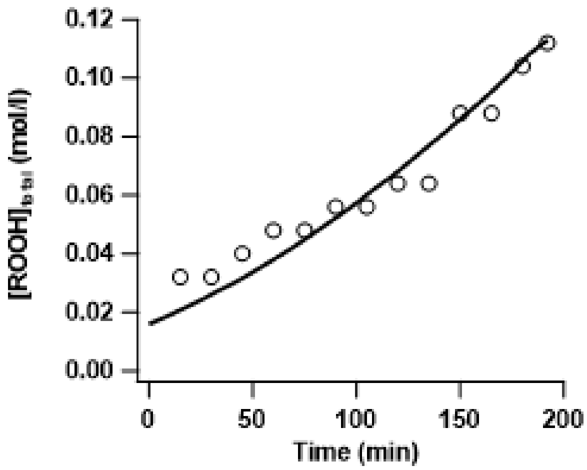

Figure 9. Simulated and measured concentrations of total hydroperoxides formed during a PetroOxy test of n-decane at 413 K and 7 bar initial of oxygen. Experimental data are given in Table S6.

The experiments show that the concentration of hydroperoxides increases with time as *n*-decane oxidation progresses. For these conditions, and within the IP time range, no extremum is observed in the [ROOH] curve as a function of time. The simulations agree with the ROOH profile measured in the PetroOxy rig. Simulations show that the formed ROOH are solely $C_{10}H_{21}OOH$. Under these conditions, the conversion of *n*-decane at the end of the test (190 minutes) reaches 3.6% and the product branching ratios are 0.76, 0.18 and 0.06 for $C_{10}H_{21}OOH$, $C_{10}H_{21}OH$ and $C_{10}H_{20}(C=O)$, respectively ($C_{10}H_{20}(C=O)$ are lumped decanones and decanals and $C_{10}H_{21}OH$ are lumped decanols). Figure S1 presents these product profiles as a function of time. The flux analysis shows that almost all C_{10} alcohols come from H-abstractions from *n*-decane by C_{10} alkoxy radicals, which are produced in the unimolecular decomposition of the $C_{10}H_{21}OOH$.

Our new kinetic model of autoxidation of *n*-decane was also compared with experimental data of the literature. Cullis et al. [17] investigated *n*-decane autoxidation in a semi-open reactor in which a flux of oxygen was passed through the liquid fuel, at a constant temperature of 423 K. Major products of *n*-decane autoxidation includes C_{10}-hydroperoxides, C_{10}-alcohols, and C_{10} carbonyls that were quantified as a function of time. Figure 10.a presents the formation of C_{10} hydroperoxides per initial mole of *n*-decane and figure 10.b illustrates the formation of sum of C_{10}-decanols and C_{10}-decanones/decanal per initial mole of *n*-decane.

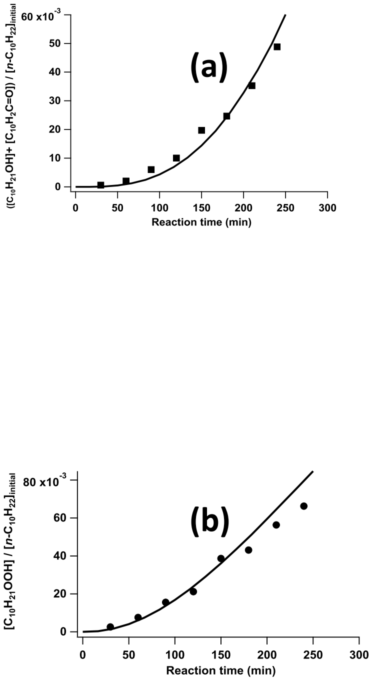

Figure 10. Simulation of products formed during the autoxidation of *n*-decane and comparison with experiments from Cullis et al. [17] at 423 K, $P_{ini, O2}$ = 700 kPa, $V_{ini, liquid}$ = 5 ml. Symbols: experiments, lines: simulations. (a): formation of C_{10}-hydroperoxides, (b): formation of C_{10}-ketones/decanal and C_{10} alcohols.

The simulation agrees with experimental results. The ratio [C_{10} alcohol] / [C_{10} carbonyls] is constant over the reaction time and is equal to 3. At a reaction time of 117 min, 3.6% of conversion is reached and the same branching ratios as those found in the simulation plotted in Figure 9 are found for $C_{10}H_{21}OOH$, $C_{10}H_{21}OH$ and $C_{10}H_{20}$(C=O) (0.76, 0.18 and 0.06). At 250 min, *n*-decane conversion is 16% and the branching ratios of $C_{10}H_{21}OOH$, $C_{10}H_{21}OH$ and $C_{10}H_{20}$(C=O) are 0.58, 0.31 and 0.10, respectively. It can be noted that water is also a major product of *n*-decane autoxidation but is not included in the latter branching ratios because it does not contain carbon atoms. The concentration of H_2O is always similar to that of $C_{10}H_{20}(C{=}O)$ in the simulations of PetroOxy experiments and of the data of Cullis et al. [17]. For example, simulated $[H_2O]$ is equal to 6.7 10^{-2} mol l^{-1} at the end of Cullis et al. experiments vs 6.67 10^{-2} mol l^{-1} for $C_{10}H_{20}(C{=}O)$.

4.2. Kinetic model analysis

4.2.1. Reaction pathways of *n*-decane autoxidation

Rate of production (ROP) analyses were carried at 413 K, $P_{ini,O2}$ = 700 kPa, $V_{ini,liq}$ = 5 mL for a conversion of *n*-decane of about 4%. Figure 11 presents the main reaction pathways of *n*-decane liquid-phase oxidation at the examined condition.

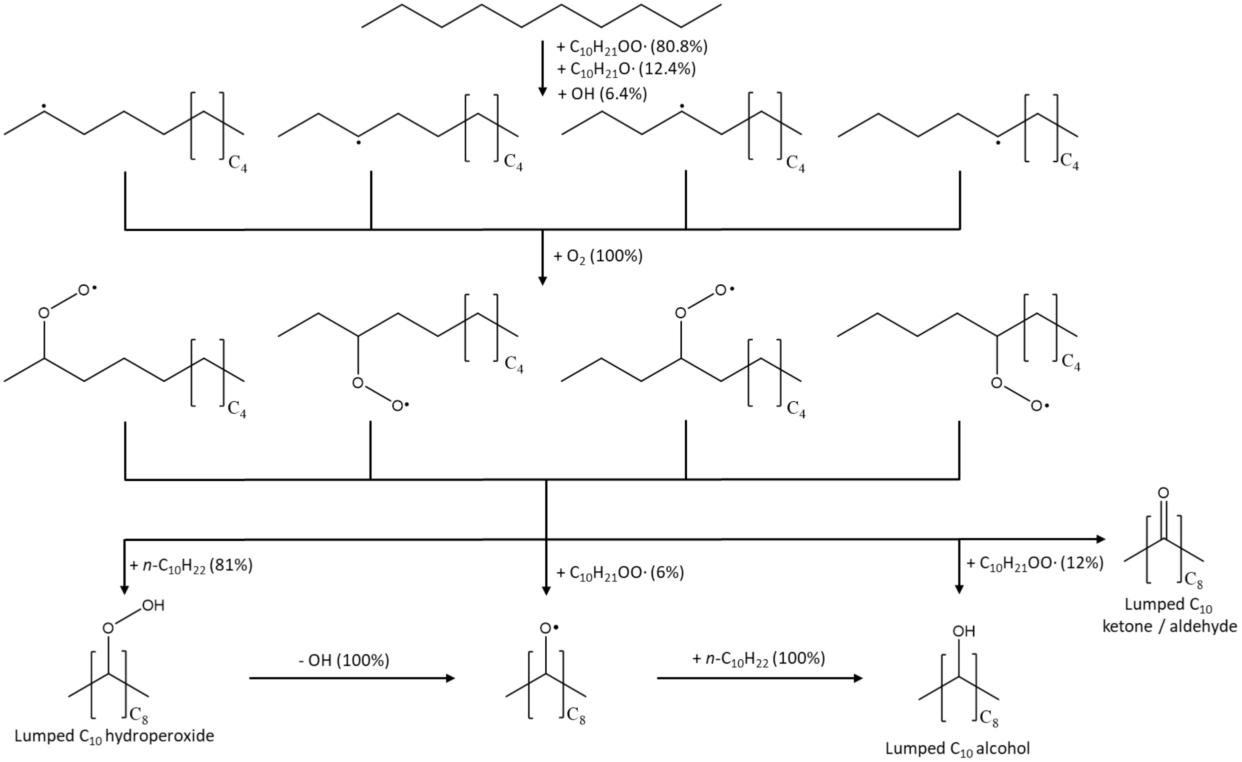

Figure 11. Reaction pathways of n-decane in the liquid phase at 413 K. ≈ 4% conversion of n-decane (190 min residence time).

The reaction scheme of *n*-decane is found to be very similar to the one of *n*-butane [26]. The main consumption flux of *n*-decane is H-atom abstractions by *n*-decyl peroxy radicals ($C_{10}H_{21}$-OO·) (80.8%), C_{10} alkoxy radicals ($C_{10}H_{21}$-O·) (12.4%), and OH (6.4%) radicals, yielding five isomers of decyl radicals. The latter radicals entirely yield decyl peroxy radicals ($C_{10}H_{21}$-OO·) through addition on O_2. The majority of decyl peroxy radicals (81%) leads to the formation of decyl hydroperoxide through H-atom abstractions from *n*-decane. The remaining part of $C_{10}H_{21}$-OO· reacts in the self-termination reactions to produce decanol ($C_{10}H_{21}$-OH), C_{10} decanone/decanal ($C_{10}H_{20}$-OK), and C_{10} alkoxy radicals ($C_{10}H_{21}$-O·). Decyl hydroperoxide decomposes into two fragments, C_{10} alkoxy radicals, and OH radicals. This reaction is the most important reactions governing the liquid-phase reactivity of *n*-decane as it transforms a neutral molecule into two reactive radicals. Sensitivity analyses presented in Figure 12 confirm the central kinetic role of this reaction. C_{10} alcohols are produced by both self-termination reactions of decyl peroxide radicals and by H-abstraction by $C_{10}H_{21}$-O· from *n*-decane. The major part of decanols is produced in the latter process. Once formed, C_{10} alcohols are principally consumed by reactions with C_{10} peroxy radicals (97.7%), through H-abstractions producing C_{10} alcohols radicals (·$C_{10}H_{20}$-OH). The latter radical is then oxidized into C_{10} carbonyl compounds by successive processes: addition of O_2, and elimination of HO_2.

4.2.2. Sensitivity analysis of the autoxidation kinetic model of *n*-decane

Sensitivity analyses have been performed to determine the most sensible reactions in an oxidation mechanism of fuel [54]. These analyses were conducted on the conversion of *n*-decane at 413 K and 7 bar initial of oxygen. Sensitivity analyses were initiated by the modification of the A-factor of the rate constant of each reaction, which was multiplied by a factor of ten. For each modification, a simulation was performed to determine the modified conversion (X_i) of *n*-decane. The sensitivity coefficient (τ_i) of each reaction was then calculated as follows:

$$\tau_i = \frac{X_i - X_0}{X_0} \times 100\ \%$$

X_0 corresponds to the simulated conversion of *n*-decane with the original unmodified model. A positive sensitivity coefficient represents a promoting effect of the considered reaction on the conversion of *n*-

decane. Conversely, a negative coefficient shows an inhibiting effect of the considered reaction on the reactivity of *n*-decane. Figure 12 summarizes the results of the sensitivity analyses.

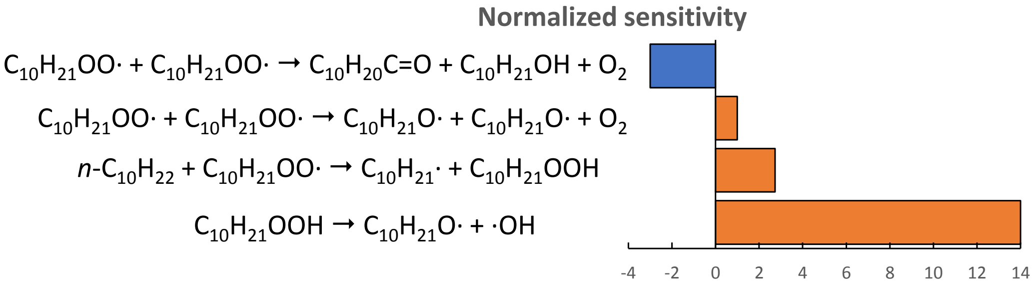

Figure 12. Sensitivity analyses on the conversion of *n*-decane during its autoxidation at 413 K

The reactions that promote the conversion of *n*-decane are H-atom abstractions from *n*-decane (*n*-$C_{10}H_{22}$) by C_{10} peroxy radicals ($C_{10}H_{21}OO\cdot$), the disproportionations of C_{10} peroxy radical producing C_{10} alkoxy radicals ($C_{10}H_{21}O\cdot$) and the decompositions of C_{10} hydroperoxide ($C_{10}H_{21}OOH$). The latter reaction has the highest promoting effect on *n*-decane conversion. The termination reactions of C_{10} peroxy radical producing C_{10} alcohols ($C_{10}H_{21}OH$) and C_{10} carbonyl compounds ($C_{10}H_{20}C{=}O$) is the most inhibiting reaction of the mechanism. The branching ratios for the reaction products of the self-termination $C_{10}H_{21}OO\cdot + C_{10}H_{21}OO\cdot$ is sensitive for the conversion of *n*-decane. In this study, the ratio of the channel '$C_{10}H_{21}O\cdot + C_{10}H_{21}O\cdot + O_2$' over the channel '$C_{10}H_{22}C{=}O + C_{10}H_{21}OH + O_2$' was fixed to a factor of 2. Further work is deserved to refine the determination of this ratio in the autoxidation of *n*-decane and other alkanes.

5. Conclusion

Experiments and modeling works were conducted to investigate the autoxidation of *n*-decane. The induction periods of *n*-decane were measured in a PetroOxy and the total hydroperoxydes content in oxidized *n*-decane was systematically quantified using colorimetric and potentiometric titrations.

Modeling works were performed to examine, in depth, the liquid-phase reactivity of *n*-decane. For the first time, a physical model was proposed to estimate liquid-phase composition at the beginning of a petroOxy experiment. Indeed, the knowledge of the liquid-phase composition is essential to rigorously simulate the autoxidation of fuels in PetroOxy experiments. A detailed kinetic model for *n*-decane oxidation in the liquid phase was developed using a state-of-the-art methodology which was developed based on solvent-adapted corrections for thermodynamic data (with an equation of state) and for the most sensitive kinetic data. Kinetic modeling shows a good agreement with experiments. The developed kinetic model is able to reproduce reliably the measured IP of *n*-decane, at different temperatures, with a mean relative deviation of 16%. The model was also able to satisfactorily simulate our new experimental profiles of hydroperoxides measured during PetroOxy tests. In addition, the kinetic model was validated against literature data, which reported experimental concentration profiles of C_{10}-hydroperoxides, C_{10}-ketones and C_{10}-alcohols during *n*-decane autoxidation.

Kinetic analyses indicate that *n*-decane autoxidation follows a classical chain mechanism applied for the liquid-phase oxidation. The main consumption pathway of *n*-decane is the H-abstraction by C_{10} peroxy radicals leading to the formation of C_{10} hydroperoxides as major products. Similar to *n*-butane autoxidation modeling, the self-reactions of peroxides radicals (ROO·) and its exit channels branching ratios play an important role in the reaction fluxes. The uncertainty of the kinetic parameters of this type of reactions remains high and deserves more studies. The proposed kinetic model is validated for limited conversions (up to about 15%) of *n*-decane. In order to expend its validity for higher conversions, the secondary mechanism needs to be further detailed.

This work contributes to the systematic understanding of the oxidation stability of *n*-decane and the validated kinetic model is a first step towards the development of a detailed kinetic model for the autoxidation of a more complex jet fuel surrogate.

Supplemental material

Simulations of products formation in a Petroxy test**,** measured IPs, pressure profiles in the PetroOxy, [ROOH] concentrations, calculations of uncertainties in [ROOH] and the simulation of product profiles as a function of time for the autoxidation of *n*-decane at 413K are given in supplemental material.

Acknowledgments

This work was financially supported by the ANR BioACe project, grant ANR-18-CE05-002 of the French National Research Agency. This project has received funding from the European Research Council (ERC) under the European Union's Horizon 2020 research and innovation program (grant agreement No 101003318). High performance computing resources were provided by the EXPLOR center hosted by the University of Lorraine. This work was also granted access to the HPC resources of IDRIS under the allocation 2022-AD010812434R1.

References

[1] Gössling S, Humpe A. The global scale, distribution and growth of aviation: Implications for climate change. Global Environmental Change 2020;65:102194.

[2] Jia T, Zhang X, Liu Y, Gong S, Deng C, Pan L, et al. A comprehensive review of the thermal oxidation stability of jet fuels. Chemical Engineering Science 2021;229:116157.

[3] Zabarnick S. Chemical kinetic modeling of jet fuel autoxidation and antioxidant chemistry. Industrial & Engineering Chemistry Research 1993;32(6):1012-7.

[4] Kabana CG, Botha S, Schmucker C, Woolard C, Beaver B. Oxidative Stability of Middle Distillate Fuels. Part 1: Exploring the Soluble Macromolecular Oxidatively Reactive Species (SMORS) Mechanism with Jet Fuels. Energy & Fuels 2011;25(11):5145-57.

[5] Harris RV. On the threshold - The outlook for supersonic and hypersonic aircraft. Journal of Aircraft 1992;29(1):10-9.

[6] Hazlett R. Thermal Oxidation Stability of Aviation Turbine Fuels. 1991.

[7] Zabarnick S, West ZJ, Arts A, Griesenbrock M, Wrzesinski P. Studies of the Impact of Fuel Deoxygenation on the Formation of Autoxidative Deposits. Energy & Fuels 2020;34(11):13814-21.

[8] Zhang C, Hui X, Lin Y, Sung C-J. Recent development in studies of alternative jet fuel combustion: Progress, challenges, and opportunities. Renewable and Sustainable Energy Reviews 2016;54:120-38.

[9] Le Dortz R, Strozzi C, Sotton J, Bellenoue M. Evaluation of the surrogates capacity to reproduce the laminar burning velocities and the sensitivity to stretching of a commercial kerosene under constant volume combustion conditions. Fuel 2021;287:119426.

[10] Naik CV, Puduppakkam KV, Modak A, Meeks E, Wang YL, Feng Q, et al. Detailed chemical kinetic mechanism for surrogates of alternative jet fuels. Combustion and Flame 2011;158(3):434-45.

[11] Mzé-Ahmed A, Hadj-Ali K, Diévart P, Dagaut P. Kinetics of Oxidation of a Synthetic Jet Fuel in a Jet-Stirred Reactor: Experimental and Modeling Study. Energy & Fuels 2010;24(9):4904-11.

[12] El-Sayah Z, Glaude P-A, Fournet R, Sirjean B. Comparison of the Effects of Different Biofuels on the Oxidation Stability of a Hydrocarbon Fuel. SAE Technical Paper 2020; 2020-01-2101.

[13] Pfaendtner J, Broadbelt LJ. Mechanistic Modeling of Lubricant Degradation. 1. Structure−Reactivity Relationships for Free-Radical Oxidation. Industrial & Engineering Chemistry Research 2008;47(9):2886-96.

[14] Jalan A, West RH, Green WH. An Extensible Framework for Capturing Solvent Effects in Computer Generated Kinetic Models. The Journal of Physical Chemistry B 2013;117(10):2955-70.

[15] Van de Vijver R, Vandewiele NM, Bhoorasingh PL, Slakman BL, Seyedzadeh Khanshan F, Carstensen H-H, et al. Automatic Mechanism and Kinetic Model Generation for Gas- and Solution-Phase Processes: A Perspective on Best Practices, Recent Advances, and Future Challenges. International Journal of Chemical Kinetics 2015;47(4):199-231.

[16] Curran HJ. Developing detailed chemical kinetic mechanisms for fuel combustion. Proceedings of the Combustion Institute 2019;37(1):57-81.

[17] Cullis C, Hirschler M, Rogers R. The oxidation of decane in the liquid and gaseous phases. Proceedings of the Royal Society of London A Mathematical and Physical Sciences 1981;375(1763):543-63.

[18] Goosen A, Morgan DH. Autoxidation of nonane and decane: a product study. Journal of the Chemical Society, Perkin Transactions 2 1994(3):557-62.

[19] Pfaendtner J, Broadbelt LJ. Mechanistic Modeling of Lubricant Degradation. 2. The Autoxidation of Decane and Octane. Industrial & Engineering Chemistry Research 2008;47(9):2897-904.

[20] Chatelain K, Nicolle A, Ben Amara A, Catoire L, Starck L. Wide Range Experimental and Kinetic Modeling Study of Chain Length Impact on n-Alkanes Autoxidation. Energy & Fuels 2016;30(2):1294-303.

[21] Gao CW, Allen JW, Green WH, West RH. Reaction Mechanism Generator: Automatic construction of chemical kinetic mechanisms. Computer Physics Communications 2016;203:212-25.

[22] Auzani AS, Clements AG, Hughes KJ, Ingham DB, Pourkashanian M. Assessment of ethanol autoxidation as a drop-in kerosene and surrogates blend with a new modelling approach. Heliyon 2021;7(6):e07295.

[23] Alborzi E, Dwyer MR, Parks CM, Sheikhansari A, Mielczarek DC, Zanganeh M, et al. Construction of a reduced chemical kinetic mechanism for autoxidation of n-paraffinic solvent – A model for aviation fuel. Fuel 2021;294:120170.

[24] Buda F, Bounaceur R, Warth V, Glaude PA, Fournet R, Battin-Leclerc F. Progress toward a unified detailed kinetic model for the autoignition of alkanes from C4 to C10 between 600 and 1200 K. Combustion and Flame 2005;142(1):170-86.

[25] Warth V, Stef N, Glaude PA, Battin-Leclerc F, Scacchi G, Côme GM. Computer-Aided Derivation of Gas-Phase Oxidation Mechanisms: Application to the Modeling of the Oxidation of n-Butane. Combustion and Flame 1998;114(1):81-102.

[26] Le MD, Warth V, Giarracca L, Moine E, Bounaceur R, Privat R, et al. Development of a Detailed Kinetic Model for the Oxidation of n-Butane in the Liquid Phase. The Journal of Physical Chemistry B 2021;125(25):6955-67.

[27] Moine E, Privat R, Jaubert J-N, Sirjean B, Novak N, Voutsas E, et al. Can we safely predict solvation Gibbs energies of pure and mixed solutes with a cubic equation of state? Pure and Applied Chemistry 2019;91(8):1295-307.

[28] Bacha K, Ben-Amara A, Vannier A, Alves-Fortunato M, Nardin M. Oxidation Stability of Diesel/Biodiesel Fuels Measured by a PetroOxy Device and Characterization of Oxidation Products. Energy & Fuels 2015;29(7):4345-55.

[29] Webster RL, Rawson PM, Kulsing C, Evans DJ, Marriott PJ. Investigation of the Thermal Oxidation of Conventional and Alternate Aviation Fuels with Comprehensive Two-Dimensional Gas Chromatography Accurate Mass Quadrupole Time-of-Flight Mass Spectrometry. Energy & Fuels 2017;31(5):4886-94.

[30] Aminane S, Sicard M, Melliti Y, Ser F, Sicard L. Experimental study of the kinetics of degradation of n-dodecane under thermo-oxidative stress at low temperature and mechanism inferred. Fuel 2022;307:121669.

[31] Duong S, Lamharess-Chlaft N, Sicard M, Raepsaet B, Galvez ME, Da Costa P. New Approach for Understanding the Oxidation Stability of Neopolyol Ester Lubricants Using a Small-Scale Oxidation Test Method. ACS Omega 2018;3(9):10449-59.

[32] Nadkarni R, Nadkarni R. Guide to ASTM test methods for the analysis of petroleum products and lubricants. ASTM International West Conshohocken; 2007.

[33] Ben Amara A, Nicolle A, Alves-Fortunato M, Jeuland N. Toward Predictive Modeling of Petroleum and Biobased Fuel Stability: Kinetics of Methyl Oleate/n-Dodecane Autoxidation. Energy & Fuels 2013;27(10):6125-33.

[34] Mielczarek DC, Matrat M, Amara AB, Bouyou Y, Wund P, Starck L. Toward the Accurate Prediction of Liquid Phase Oxidation of Aromatics: A Detailed Kinetic Mechanism for Toluene Autoxidation. Energy & Fuels 2017;31(11):12893-913.

[35] Roohi H, Rajabi M. Iodometric Determination of Hydroperoxides in Hydrocarbon Autoxidation Reactions Using Triphenylphosphine Solution as a Titrant: A New Protocol. Industrial & Engineering Chemistry Research 2018;57(20):6805-14.

[36] Morris RE, Black BH, Mitchell CS. AN IMPROVED METHOD FOR MEASURING HYDROPEROXIDES IN FUEL USING POTENTIOMETRY AND ALTERNATIVES TO CHLOROFLUOROCARBON SOLVENTS. Fuel Science and Technology International 1994;12(7-8):1003-18.

[37] West ZJ, Zabarnick S, Striebich RC. Determination of Hydroperoxides in Jet Fuel via Reaction with Triphenylphosphine. Industrial & Engineering Chemistry Research 2005;44(10):3377-83.

[38] Giarracca L, Isufaj F, Lizardo-Huerta JC, Fournet R, Glaude PA, Sirjean B. Experimental and kinetic modeling of the ignition delays of cyclohexane, cyclohexene, and cyclohexadienes: Effect of unsaturation. Proceedings of the Combustion Institute 2021;38(1):1017-24.

[39] Schönborn A, Le MD, Fournet R, Glaude P-A, Warth V, Sirjean B. Auto-ignition control using an additive with adaptable chemical structure. Part I: Development of a kinetic model for 1,3-cyclohexadiene and 1,3,5-hexatriene combustion. Combustion and Flame 2019;205:466-83.

[40] Schönborn A, Le MD, Fournet R, Glaude P-A, Warth V, Sirjean B. Autoignition Control Using an Additive with Adaptable Chemical Structure. Part 2. Development of a PRF Kinetic Model Including 1,3-Cyclohexadiene Mechanism and Simulations of Ignition Control. Energy & Fuels 2019;33(12):12704-13.

[41] Bounaceur R, Glaude P-A, Sirjean B, Fournet R, Montagne P, Vierling M, et al. Prediction of Auto-Ignition Temperatures and Delays for Gas Turbine Applications. Journal of Engineering for Gas Turbines and Power 2015;138(2).

[42] Lizardo-Huerta J-C, Sirjean B, Glaude P-A, Fournet R. Pericyclic reactions in ether biofuels. Proceedings of the Combustion Institute 2017;36(1):569-76.

[43] Muller C, Michel V, Scacchi G, Côme G-M. THERGAS: a computer program for the evaluation of thermochemical data of molecules and free radicals in the gas phase. Journal de chimie physique 1995;92:1154-78.

[44] Benson SW, Cruickshank FR, Golden DM, Haugen GR, O'Neal HE, Rodgers AS, et al. Additivity rules for the estimation of thermochemical properties. Chemical Reviews 1969;69(3):279-324.

[45] Voutsas E, Louli V, Boukouvalas C, Magoulas K, Tassios D. Thermodynamic property calculations with the universal mixing rule for EoS/GE models: Results with the Peng–Robinson EoS and a UNIFAC model. Fluid Phase Equilibria 2006;241(1):216-28.

[46] Moine E, Privat R, Sirjean B, Jaubert J-N. Estimation of solvation quantities from experimental thermodynamic data: Development of the comprehensive CompSol databank for pure and mixed solutes. Journal of Physical and Chemical Reference Data 2017;46(3):033102.

[47] Denisov ET, Afanas' ev IB. Oxidation and antioxidants in organic chemistry and biology. CRC press, Boca Raton; 2005.

[48] Emanuel NM. THE PROBLEM OF THE CONTROL OF THE CHAIN REACTIONS TAKING PLACE IN THE LIQUID-PHASE OXIDATION OF HYDROCARBONS. In: Emanuel NM, editor The Oxidation of Hydrocarbons in the Liquid Phase. Pergamon; 1965, p. 1-31.

[49] Dixon KW. Decomposition Rates of Organic Free Radical Initiators. The Wiley Database of Polymer Properties. 2003.

[50] Rowley R. DIPPR^(! R) Data Compilation of Pure Chemical Properties. Design Institute for Physical Properties 2010.

[51] Holderbaum T, Gmehling J. PSRK: A group contribution equation of state based on UNIFAC. Fluid Phase Equilibria 1991;70(2-3):251-65.

[52] Baudouin O, Dechelotte S, Guittard P, Vacher A. Simulis® Thermodynamics: an open framework for users and developers. Computer Aided Chemical Engineering. Elsevier; 2008, p. 635-40.

[53] Kee RJ, Rupley FM, Miller JA. Chemkin-II: A Fortran chemical kinetics package for the analysis of gas-phase chemical kinetics. Sandia National Lab.(SNL-CA), Livermore, CA (United States); 1989.

[54] Le MD, Matrat M, Amara AB, Foucher F, Moreau B, Yu Y, et al. Experimental and numerical investigation of the promoting effect of a cetane booster in a low-octane gasoline fuel in a rapid compression machine: A study of 2-ethylhexyl nitrate. Combustion and Flame 2020;222:36-47.